
EXTENDING THE HANDOVER-ITERATIVE VQE TO CHALLENGING STRONGLY CORRELATED SYSTEMS: N_2 AND FE-S CLUSTER

Pilsun Yoo¹, Kyungmin Kim¹, Eyuel E. Elala¹, Shane McFarthing¹, Aidan Pellow¹, Johanna I. Fuks¹, Doo Hyung Kang¹, Pratanaphorn Nakliang¹, Jaewan Kim¹, Himadri Pathak², Tomonori Shirakawa², Seiji Yunoki², and June-Koo Kevin Rhee^{1,*}

¹Qunova Computing, Inc., Daejeon, Rep. of Korea

²RIKEN, Kobe, Japan

January 13, 2026

ABSTRACT

Accurately describing strongly correlated electronic systems remains a central challenge in quantum chemistry, as electron–electron interactions give rise to complex many-body wavefunctions that are difficult to capture with conventional approximations. Classical wavefunction-based approaches, such as the Semistochastic Heat-bath Configuration Interaction (SHCI) and the Density Matrix Renormalization Group (DMRG), currently define the state of the art, systematically converging toward the Full Configuration Interaction (FCI) limit, but at a rapidly increasing computational cost. Quantum computing algorithms promise to alleviate this scaling bottleneck by leveraging entanglement and superposition to represent correlated states more compactly. We introduced the Handover-Iterative Variational Quantum Eigensolver (HI-VQE) as a practical quantum computing algorithm with an iterative “handover” mechanism that dynamically exchanges information between quantum and classical computers, even using Noisy Intermediate-Scale Quantum (NISQ) computers. In this work, we extend the HI-VQE to benchmark two prototypical strongly correlated systems, the nitrogen molecule (N_2) and iron–sulfur (Fe–S) cluster, which serve as stringent tests for both classical and quantum electronic-structure methods. By comparing HI-VQE results against Heat-bath Configuration Interaction (HCI) benchmarks, we assess its accuracy, scalability, and ability to capture multireference correlation effects. Achieving quantitative agreement on these canonical systems demonstrates a viable pathway toward quantum-enhanced simulations of complex bioinorganic molecules, catalytic mechanisms, and correlated materials.

1 Introduction

Quantum mechanics provides an exceptionally accurate description of the microscopic world, as demonstrated by its precise prediction of experiments[1–3]. Quantum phenomena are at the heart of many modern technologies and are omnipresent in chemistry and materials science. However, simulating systems of industrial or technological relevance remains a formidable challenge, owing to the exponential growth of Hilbert space as 2^N with the number of particles (atoms and electrons) involved. Despite continuous advances in high-performance computing, parallelization, and GPU acceleration, the exact solution of the Schrödinger equation remains feasible only for systems comprising a few tens of electrons[4, 5]. This limitation has motivated the development of different types of first-principles electronic-structure methods that approximate the electronic densities or wavefunctions, typically represented in a complete set of independent orbitals serving as basis functions. Among first-principles approaches, Density Functional Theory (DFT) has become the most widely used method for simulating the electronic degrees of freedom that govern chemical reactivity, owing to its favorable balance between accuracy and computational efficiency. This efficiency enables DFT to handle systems containing thousands of atoms[6]. However, systems exhibiting strong electronic correlations

pose a major challenge for density functional approximations[7–9]. Among single-reference wavefunction methods, Coupled Cluster with Singles, Doubles and Triples (CCSD(T)) is widely regarded as the gold standard in quantum chemistry; nevertheless, it also fails to capture the multireference character associated with strong correlation[10, 11]. Thus, achieving a reliable description of electron correlation remains one of the central challenges in the field[12, 13]. Transition metals and stretched molecules are prototypical examples of strongly correlated systems, where several electronic configurations contribute comparably to the ground state and cannot be described by a single reference. The dissociation of the nitrogen molecule (N_2) and iron–sulfur (Fe–S) clusters are among the most stringent and informative benchmarks for multireference methods. These systems exemplify distinct yet complementary correlation challenges: N_2 is the archetypal case of bond dissociation and static correlation, while Fe–S clusters manifest multi-center spin coupling and charge delocalization.

Multireference methods replace the single-determinant reference with a multideterminantal one built from correlated orbitals. In the complete active space (CAS) approach the orbital space is partitioned into three spaces: an inactive space with doubly occupied orbitals, a virtual space with unoccupied orbitals, and an active space in which all possible occupation are considered. The CAS number (number of determinants in the active space) grows combinatorially with the number of active electrons and orbitals, but many of these determinants contribute minimally to the accuracy of the final electronic wave function and energy. Selected configuration interaction (SCI) methods exploit this by selecting only the important determinants, and often refine the variational energy with a multireference perturbative correction (SCI+PT methods). Among SCI+PT approaches, the heat-bath configuration interaction (HCI) method has proven particularly effective, achieving sub-millihartree accuracy in variational spaces containing up to 10^{20} determinants [14]. HCI generates single and double excitations from a reference state and selects the determinants with Hamiltonian matrix element above a given threshold ϵ . The stochastic heat-bath configuration interaction (SHCI) method combines this deterministic selection of determinants with large Hamiltonian couplings with a stochastic perturbative correction, allowing millihartree accuracy for active spaces of over 100 orbitals. [15] In parallel, tensor-network formalisms, notably the Density Matrix Renormalization Group (DMRG) reformulates the wavefunction as a matrix product state (MPS) and optimizes it variationally to capture localized entanglement efficiently, yielding accurate energies in active spaces over 100 orbitals[16–20]. Together, SHCI and DMRG define the gold standard for high-accuracy classical simulations of strongly-correlated electrons, against which emerging quantum algorithms can be meaningfully benchmarked[21].

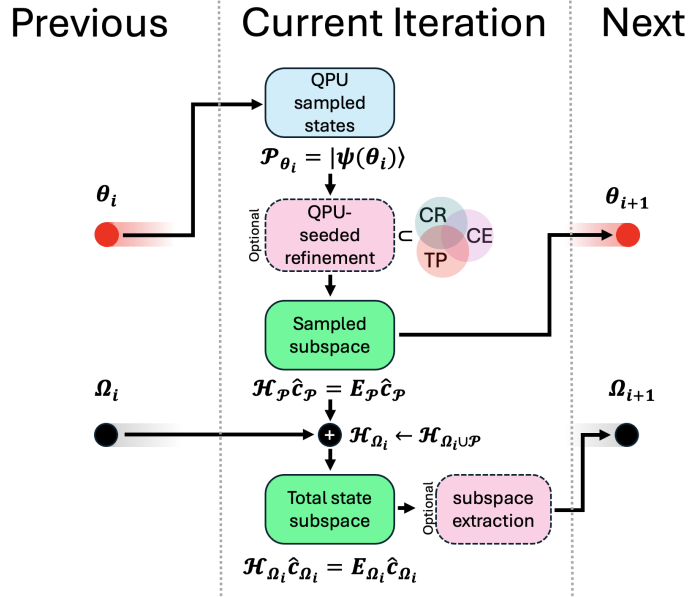


Figure 1: Overview of the HI-VQE iterative workflow. Each iteration uses QPU-sampled states with the current circuit parameters, optionally refines them via configuration recovery (CR)/tensor product (TP)/classical expansion (CE), and diagonalizes both the sampled and accumulated subspaces to update parameters and propagate the optimized state forward. The subspace extraction is optionally activated to carry on highly contributing states.

Quantum computing introduces a native platform for representing and manipulating correlated many-electron wavefunctions, offering a pathway beyond the limitations of classical scaling. The present generation of quantum devices, commonly referred to as Noisy Intermediate-Scale Quantum (NISQ) or pre-fault-tolerant processors, remains con-

strained in both circuit depth and qubit count due to decoherence, gate infidelity, and noise accumulation [22–24]. But hardware capabilities continue to advance rapidly, and universal, programmable superconducting processors now support increasingly deep and complex quantum circuits [23, 24]. In parallel, progress toward quantum advantage is driven not only by hardware development, but also by algorithmic innovation, improved resource efficiency, and better orchestration between classical and quantum computational resources [25–27]. In this context, hybrid quantum–classical algorithms have emerged as a promising strategy to leverage the strengths of both paradigms: state preparation and sampling on quantum processors, combined with optimization and error mitigation on classical hardware[25, 28, 29].

The Variational Quantum Eigensolver (VQE) is the most popular hybrid quantum–classical algorithm, in which the correlated wavefunction is prepared by quantum hardware and classical optimization is used to minimize energy[28, 30, 31]. The idea of leveraging quantum devices to guide classical subspace diagonalization has recently been explored for strongly correlated systems through extended sample-based quantum diagonalization on a quantum-centric architecture[29, 32]. Expanding this framework, the Handover Iterative Variational Quantum Eigensolver (HI-VQE)[33] introduces an iterative “handover” mechanism between quantum and classical solvers. In this approach, the quantum device identifies important electronic configurations (Slater determinants), and the classical processor refines their coefficients via subspace diagonalization. Through successive expansion and screening of the determinant space, HI-VQE achieves rapid convergence toward chemically accurate energies using a fraction of the resources required by conventional adaptive or full VQE methods. Benchmark applications to molecules such as NH_3 , Li_2S , and N_2 have demonstrated HI-VQE’s ability to reproduce high-level CASCI, HCl, or DMRG results while maintaining robustness against noise and barren-plateau effects [33].

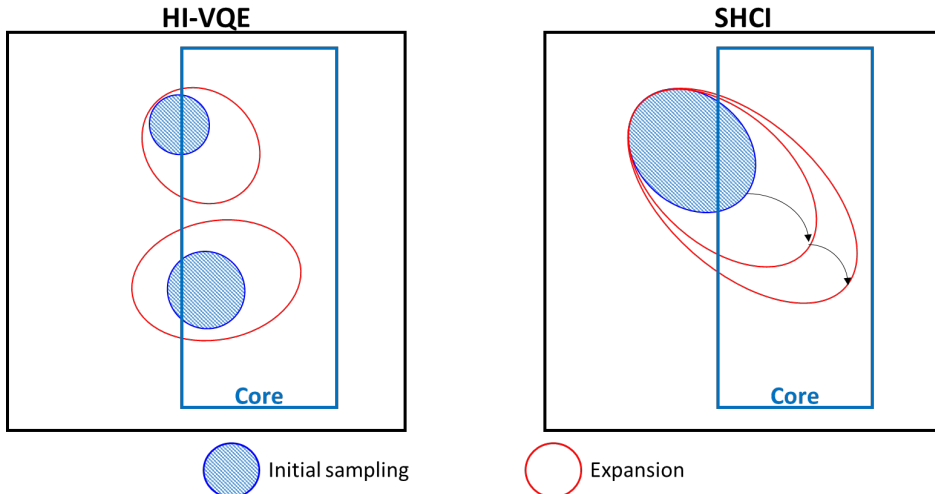


Figure 2: Subspace expansion behavior of left) HI-VQE, and right) HCl

In this work, we extend the HI-VQE framework and benchmark it on two prototypical examples of strongly correlated systems : the dissociation of the triple bond in N_2 and the Fe–S cluster ($[\text{Fe}_2\text{S}_2(\text{SCH}_3)_4]^{2-}$). By benchmarking HI-VQE against HCl [14] calculations, we assess both its quantitative accuracy and its ability to identify the electronic configurations most relevant for capturing correlation. We analyze the compactness and quality of the determinant subspace selected by HI-VQE and compare it with that of HCl across different correlation regimes. Reliable reproduction of classical benchmark results on these problems paves the way for quantum-enhanced approaches to complex bioinorganic, catalytic, and strongly correlated materials problems, marking a promising step toward demonstrating quantum advantage as hardware capabilities continue to advance.

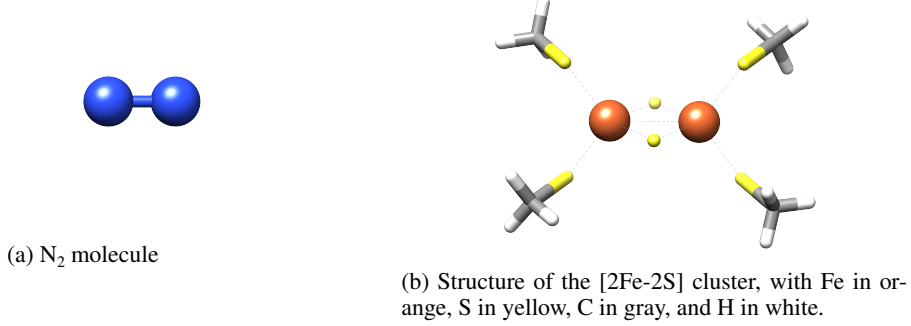
2 Methods

2.1 Details for Molecular System

The molecules simulated in this work are summarized in Table 1. The dissociation of N_2 is studied using the cc-pVDZ basis and an all-electron active space with (14e,28o). As a classical reference, the potential energy curve was computed using the HCl method. The molecular geometry and active space selection of the $[\text{Fe}_2\text{S}_2(\text{SCH}_3)_4]^{2-}$ cluster (denoted as [2Fe–2S]) used in this work was adopted from Robledo-Moreno et al. 2025 [29]. This ensures that our computational results remain directly comparable to the benchmarking data reported in that study, facilitating a rigorous assessment

of the accuracy and convergence of the method. Specifically, the atomic coordinates of the [2Fe–2S] cluster were taken as reported in [34] and the active space was selected using the procedure described in [35] and available on the SQD data repository[36].

Table 1: Chemical systems and their computational parameters



Chemical Systems	Active Space	CAS size	No. of Qubits	Basis Set
N_2	(14e,28o) ^a	1.40×10^{12}	56	cc-pVDZ
$[\text{Fe}_2\text{S}_2(\text{SCH}_3)_4]^{2-}$	(30e,20o)	2.40×10^8	40	TZP-DHK

^a all-electron calculation

2.2 Algorithmic details of HI-VQE

The algorithmic implementation closely follows the HI-VQE formulation presented in [33], with several refinements introduced to improve computational efficiency for systems exceeding 40 qubits. Figure 1 presents an overview of the iterative workflow, in which QPU-sampled states are incorporated into the evolving subspaces, with an optional configuration-recovery step, and then diagonalized to update the circuit parameters at each iteration. For the quantum Ansatz of simulations, an Excitation-Preserving Ansatz (EPA) with linear entanglement topology was employed, incorporating between two and four repetitions of the quantum circuit to vary the excitation levels of the electronic configurations. This structure ensures particle-number and spin conservation while maintaining manageable circuit depth for large-scale simulations. For the handover computations, a modified sparse matrix diagonalization procedure was implemented for the calculation of the selected configuration interaction (SCI), based on the Arrow SHCI code [14, 15, 37]. The code was adapted to perform a single HCI expansion using the supplied electronic configuration states, and to compute spin-resolved reduced density matrices (RDMs) from the diagonalization results. These modifications enable efficient handling of both the sampled and total state spaces within HI-VQE. All QPU samplings are currently carried out on the `ibm_fez` backend, with the number of shots per iteration ranging from 2,000 to 500,000, depending on the convergence behavior and system size. The configuration recovery protocol, proposed in [29], was incorporated as an error mitigation step for noisy QPU samples. This procedure corrects invalid electronic configurations by referencing the electronic occupation numbers determined from the diagonalization of the core state in the preceding iteration. For the initial iteration, the Hartree-Fock occupation numbers or another designated reference state were used as the baseline for correction. Finally, the amplitude truncation scheme based on CI coefficients introduced in the HI-VQE manuscript was applied to both sampled and total states under distinct criteria. For the sampled states, configurations were sorted by the squared CI coefficients, and only the top-ranked states—up to a user-defined limit—were retained. In contrast, truncation of the total states was performed using the squared CI coefficients without imposing a fixed limit on the number of accumulated states, allowing the progressive construction of carry-over core states across iterations.

2.3 Calculation details for HI-VQE

This section summarizes the key computational settings used for all HI-VQE simulations carried out in this work. All quantum-sampling procedures were executed on the `ibm_fez` backend of the IBM Quantum platform, covering molecular systems ranging from 24 to 56 qubits. Table 2 provides a detailed overview of the configuration employed for each benchmark, including the backend, number of measurement shots, qubit counts, ansatz types, and the number of independent HI-VQE calculations performed.

The N_2 cc-pVDZ benchmarks consist of two categories: (i) 56-qubit Potential Energy Surface (PES) calculations used to investigate dissociation behavior (N_2 :(Dist,Energy)), and (ii) variable-qubit studies (24–56 qubits) designed to examine determinant number growth and resource scaling denoted as N_2 :(Qubits,Dets). For the [2Fe-2S] cluster, we evaluated the effect of measurement noise using 50,000-shot ([2Fe-2S]:case_1) and 100,000-shot ([2Fe-2S]:case_3) simulations. In addition, the 50,000-shot case was used to compare two quantum Ansätze for feasibility assessment: the EPA-L-R2 excitation-preserving Ansatz ([2Fe-2S]:case_1) and a tailored *ad hoc* circuit ([2Fe-2S]:case_2). The EPA-L-R2 denotes an excitation-preserving Ansatz with linear entanglement and two repetitions of the circuit block.

Table 2: Molecular structures and Parameters for HI-VQE calculations

Calculation type	Backend	No. of Shot	No. of Qubit	Ansatz	No. of Calculations
N_2 :(Dist,Energy)	<code>ibm_fez</code>	4,000	56	EPA-L-R2	9
N_2 :(Qubits,Dets)	<code>ibm_fez</code>	4,000	24–56	EPA-L-R2	9
[2Fe-2S]:case_1	<code>ibm_fez</code>	50,000	40	EPA-L-R2	3
[2Fe-2S]:case_2	<code>ibm_fez</code>	50,000	40	<i>Ad hoc</i>	3
[2Fe-2S]:case_3	<code>ibm_fez</code>	100,000	40	<i>Ad hoc</i>	1
[2Fe-2S]:case_4	<code>ibm_fez</code>	25,000	40	<i>Ad hoc</i>	1

3 Results and Discussion

3.1 Dissociation of Nitrogen molecule (N_2)

The N_2 dissociation curve in the cc-pVDZ basis remains a textbook test for multireference accuracy, as the system transitions from a single-reference description near equilibrium to a highly degenerate manifold at large bond separations.[38, 39] Capturing this transition continuously and quantitatively remains a benchmark of any correlated-electron approach, classical or quantum. Near the equilibrium bond distance, the CCSD and CCSD(T) methods yield potential energies close to experimental dissociation energies due to a well-described dynamic correlation. However, as the N-N bond elongates toward dissociation, the single-reference wavefunction underlying CCSD and CCSD(T) becomes inadequate since it can not describe separated fragments with localized spins, leading to a systematic overestimation of the energy and a failure to capture static correlation effects from near-degenerate electronic configurations. [11, 40, 41]. Standard density-functional approximations also suffer from the inability to describe systems with fractional spins and fail to reproduce molecular dissociation curves (including N_2) due to strong static correlation and delocalization errors.[42, 43] This highlights a central lesson in quantum chemistry that method choice must track the evolving electron correlation character along the entire PES. In Table 4, the experimental dissociation energy of N_2 is compared to the numerical estimations obtained with different computational methods. The dissociation energy was estimated from $E_{diss} = E_{extended} - E_{eq}$ for the computational approaches.

Table 3: Comparison of HI-VQE and HCI Energies along the N-N distances

N-N distances (Å)	HI-VQE Energy (Ha)	HCI Energy (Ha)		ΔE^a (mHa)
		$\epsilon = 2 \times 10^{-6}$	$\epsilon = 1 \times 10^{-6}$	
0.90	-109.0625337	-109.062579	-109.062600	0.0667
0.80	-108.6659061	-108.665944	-108.665961	0.0552
1.00	-109.2322559	-109.232352	-109.232376	0.1197
1.10	-109.2810451	-109.281095	-109.281122	0.0771
1.20	-109.2684836	-109.268547	-109.268575	0.0910
1.50	-109.1284202	-109.128515	-109.128547	0.1268
2.00	-108.9849804	-108.985157	-108.985189	0.2083
2.50	-108.9640293	-108.964173	-108.964199	0.1698
3.00	-108.9612287	-108.961473	-108.961496	0.2675

^a $E_{HI-VQE} - E_{HCI(\epsilon=1 \times 10^{-6})}$

The performance of the HI-VQE for the N_2 potential energy surface was systematically investigated by benchmarking against HCI energies throughout the dissociation coordinates. Figure 3 (top panel) presents the potential energy surfaces (PES) for N_2 as calculated by both HCI (purple) and HI-VQE (yellow points) over a range of N–N bond distances (0.8 - 3.0 Å). The data demonstrate excellent agreement between the two methods, and HI-VQE successfully

captures both the equilibrium and the dissociation regime of the PES. The lower panel of Figure 3 quantifies the absolute errors of the HI-VQE energies relative to HCl at each bond length, expressed in millihartree (mHa). The HI-VQE method achieves agreements with HCl well below the millihartree, as shown in Table 3. This is a key benchmark, indicating that HI-VQE not only reproduces quantitative energetics at equilibrium but also maintains high fidelity across the full dissociation curve, an essential capability for accurately modeling bond breaking and strong electron correlation.

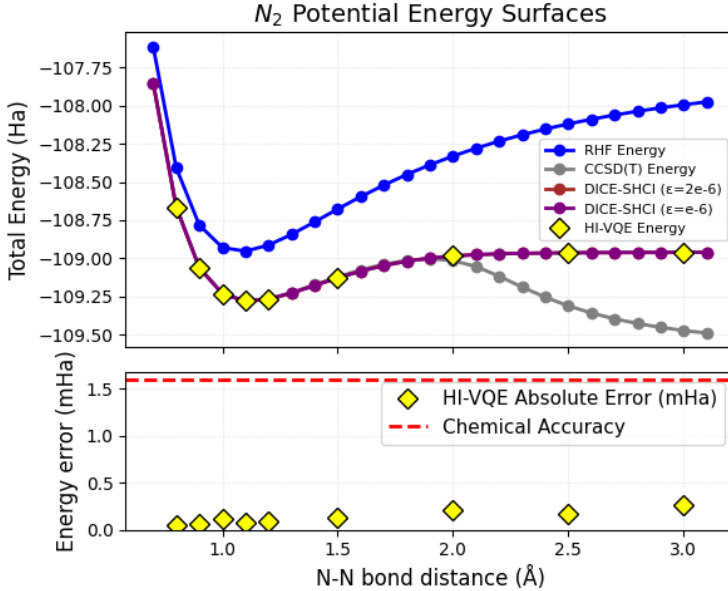


Figure 3: Top: Potential energy surface of N₂ cc-pVDZ calculated by RHF, HCl and HI-VQE. Bottom: HI-VQE energy error w.r.t. HCl ($\epsilon = 1 \times 10^{-6}$)

In the strongly correlated stretched regime, the multireference character of the wavefunction requires a larger number of determinants for an accurate representation. These determinants must be carefully selected to capture the correlation effects. In Figure 4, the subspace size (i.e., the number of determinants or electronic configurations) is shown as a function of the bond length. HI-VQE consistently operates with a significantly reduced subspace size compared to HCl at all distances. At stretched bond lengths (e.g., 3.00 Å), the computational burden for HCl escalates sharply, requiring subspaces approaching 4.5×10^7 , whereas HI-VQE maintains a substantially lower resource demand. These results indicate that HI-VQE performs a more physically meaningful and compact selection of contributing determinants in the strongly correlated regime compared to HCl.

Table 4: N₂ dissociation energy from experiments and different computational approaches

Method	Dissociation energy (eV)
Experiment ^a	9.75(6)
HF cc-VDZ ^b	26.12
DFT B3LYP cc-pVQZ ^{c,d}	> 16
CCSD(T) cc-pVDZ ^{b,d}	–
HCl cc-pVDZ ^d	8.70
HI-VQE cc-pVDZ ^d	8.70

^a Ref. [44, 45]

^b Ref. [42]

^c Ref. [40]

^d Estimated by $E_{\text{diss}} = E_{\text{Extended}} - E_{\text{eq}}$

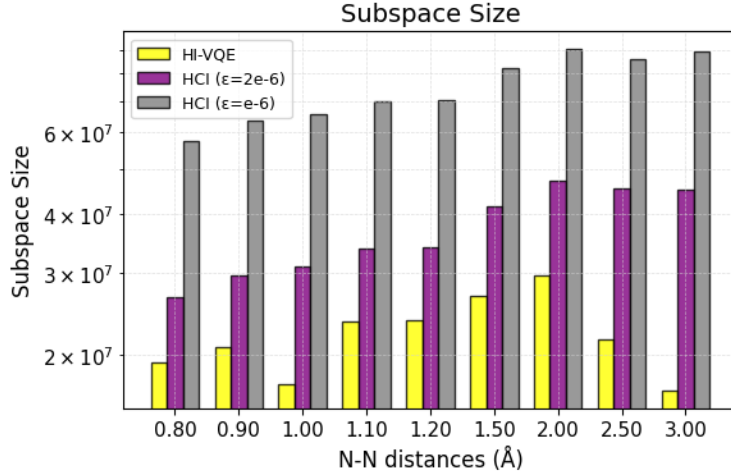


Figure 4: N_2 cc-pVDZ dissociation: subspace size comparison between HCI and HI-VQE.

3.2 Efficient Wavefunction Approximation using HI-VQE

SCI methods, including HCI, rely on a hierarchical tree search in which configurations are generated by applying increasing excitation ranks to a single reference determinant, typically Hartree–Fock. Although SCI achieves better practical scaling than FCI, often exhibiting sub-exponential growth of the selected subspace, the search process is fundamentally constrained by the sparse nature imposed by the Slater–Condon rules. Each determinant is meaningfully connected only to a limited set of other determinants through single and double excitations, creating a sparse and shallow connectivity graph. As a result, important determinants that lie far from the HF reference in excitation space, and which are crucial to describe strongly correlated multireference regimes [46], are difficult to reach through this restricted excitation tree. The method must therefore evaluate many candidate excitations at each level. The number of accessible configurations grows combinatorially with system size. This makes it increasingly difficult to efficiently identify a compact yet high-weight determinant set. By contrast, HI-VQE leverages QPU samples to directly probe the structure of the correlated wavefunction. The QPU generates excited electronic configurations without being restricted to excitation rank or proximity to the reference states, enabling expanded determinant sets to be seeded directly from measured bitstrings. As a result, HI-VQE naturally uncovers a more compact and physically relevant determinant subset by avoiding the tree-search bottleneck intrinsic to classical SCI methods.

The Complete Active Space (CAS) determinant count (CAS number) grows combinatorially and rapidly becomes intractable as the number of spin orbitals (or qubits) increases ($\binom{28}{7} = 1.4 \times 10^{12}$), as shown in Figure 5. To investigate the scaling in a controlled setting, we examined the dissociated N_2 molecule at $R = 3.0\text{\AA}$, varying the number of spin orbitals while keeping the number of electrons fixed (14 electrons). Classical HCI constructs its selected space by expanding a hierarchical excitation tree from a single reference determinant, which leads to a steep increase in the number of selected determinants as the system size grows. However, HI-VQE maintains a substantially more compact determinant representation: both the total QPU-sampled configurations and the extracted configurations from QPU-sampled configurations with amplitude screening remain one to two orders of magnitude smaller than HCI across the full qubit range. It is important to note that the HCI results shown here were carefully converged to achieve energies comparable to those of HI-VQE. These observations demonstrate that QPU sampling can efficiently identify high-weight determinants without relying on exhaustive tree search, enabling scalable many-body approximations at qubit sizes where classical SCI approaches its computational limits. Moreover, because the diagonalization cost scales as $O(N^3)$ with respect to the number of configurations N , the compact determinant space generated by HI-VQE translates directly into significantly more efficient computation within the quantum–classical hybrid framework.

The robustness of HI-VQE in this challenging regime highlights its potential as a practical quantum-classical hybrid algorithm for strongly correlated molecular systems. As N_2 dissociation represents a prototypical test of multireference correlation, the ability of HI-VQE to accurately reproduce HCI-quality results in both equilibrium and dissociated limits demonstrates its suitability for more complex systems, such as transition metal clusters and catalytic reaction paths.

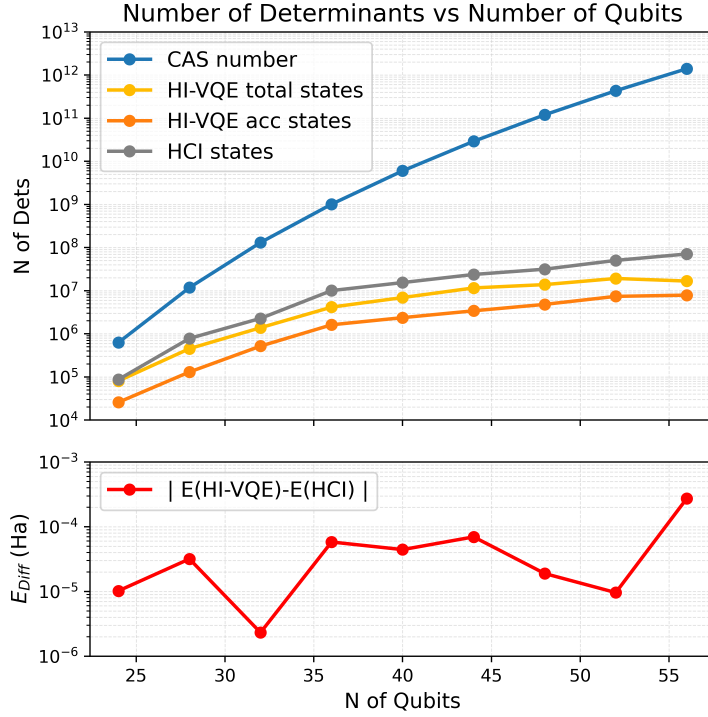


Figure 5: Top: Determinant scaling with qubit number comparison between CASCI, HI-VQE, and HCI methods for N_2 cc-pVDZ at bond distance 3.0 Å. Bottom: Absolute energy difference between HI-VQE and HCI.

Table 5: [Fe-S] cluster in TZP-DHK basis: Ground state energy, energy error and number of determinants for Hartree-Fock, CCSD, HCI and HI-VQE compared to CASCI reference.

Method	E_{total} (Ha)	ΔE^a (mHa)	No. of Dets
Hartree-Fock	-116.205816	399.7930	1
CCSD ^b	-116.405662	199.7473	-
HCI(30e,20o) ^b	-116.604878	0.7310	56,665,658
HCI(30e,20o) ^c	-116.605333	0.2760	97,503,808
HCI(30e,20o) ^d	-116.605409	0.2000	196,112,016
CASCI(30e,20o)	-116.605609	0.0000	240,374,016
HI-VQE (30e,20o)			
case_1.1	-116.604576	1.0332	66,861,907
case_1.2	-116.604682	0.9269	65,456,175
case_1.3	-116.604779	0.8298	63,857,547
case_2.1	-116.604742	0.8666	71,377,177
case_2.2	-116.604536	1.0727	64,449,164
case_2.3	-116.604543	1.0660	66,330,225
case_3	-116.601723	3.8859	53,871,015
case_4	-116.604694	0.9151	72,558,573

^a $E_m - E_{CASCI}$

^b Arrow-HCI with $\epsilon = 5 \times 10^{-6}$

^c Arrow-HCI with $\epsilon = 2 \times 10^{-6}$

^d Ref. [29]

3.3 Fe-S clusters

In contrast to N_2 , Fe-S clusters such as [2Fe-2S], [4Fe-4S], and the FeMo cofactor (FeMoco) in nitrogenase enzymes pose a far more complex problem. These clusters, composed of multiple high-spin Fe centers bridged

by sulfides, are central to numerous biological processes, including electron transfer, enzymatic catalysis, and nitrogen fixation.[34, 47–49] Beyond their biological relevance, Fe–S clusters also underpin emerging applications in biomimetic catalysis, materials design, and quantum sensing further amplifying the need for scalable, accurate electronic-structure solutions. Fe–S clusters serve, therefore, as realistic and chemically meaningful benchmarks for testing next-generation correlated-electron methodologies.[50, 51] Their dense manifolds of low-lying spin states arise from strong exchange coupling and orbital delocalization, often requiring active spaces of 60–100 orbitals or more to capture essential physics.[49, 52] Conventional single-reference approaches such as DFT and coupled-cluster theory (e.g., CCSD(T)) often fail to capture the multireference character intrinsic to Fe–S systems, particularly in low-spin or mixed-valence configurations [8, 9, 53]. To achieve quantitative accuracy, it is necessary to employ multireference wavefunction methods that can systematically recover both static and dynamic correlation within a large active space. Among classical methods, SHCI, CASCI, and DMRG are widely recognized for their capacity to address the multireference character within large active spaces required for Fe–S clusters. [29, 34, 51, 52] In Fe–S clusters, SHCI has demonstrated remarkable effectiveness in capturing ground and excited state correlation energies together with the self-consistency field (SCF) approach for orbitals optimization. [54] Recent studies show that the energy differences between SHCI and DMRG on Fe–S clusters often approach 1 millihartree, suggesting that both methods can achieve near-exact results when convergence is carefully controlled. [15, 55]

From a theoretical standpoint, Fe–S clusters represent an extreme case of multireference spin frustration.[35, 50, 51] Each Fe ion contributes a substantial local magnetic moment, yet the total cluster spin is often low due to antiferromagnetic coupling between centers. This interplay of localized and delocalized correlation renders classical FCI or multiconfigurational methods computationally prohibitive. For example, even the [2Fe–2S] cluster, a seemingly simple model, exhibits a singlet ground state emerging from intricate superexchange interactions among spin-coupled and charge-delocalized configurations. The electronic ground state of the [2Fe–2S] cluster consists of two Fe(III) centers with high-spin that are antiferromagnetically coupled. Capturing such phenomena with quantitative accuracy lies beyond the reach of conventional approaches, motivating the exploration of hybrid and quantum-assisted frameworks.

The benchmarking of the Fe–S cluster using the HI-VQE algorithm reveals a compelling balance between accuracy and computational efficiency. Table 5 highlights the performance of HI-VQE relative to classical methods such as Hartree–Fock, CCSD, and HCI. While Hartree–Fock and CCSD exhibit large deviations from the CASCI reference, underscoring their inability to capture strong correlation, HCI achieves near-exact results, but at the cost of tens to hundreds of millions of determinants. In contrast, HI-VQE reproduces HCI-level accuracy (0.83 - 3.89 mHa), while requiring roughly one-third fewer determinants (~50–70 million determinants). This reduction in determinant count demonstrates the efficiency of quantum-informed sampling in constructing a compact yet physically meaningful subspace, positioning HI-VQE as a scalable alternative for large and multireference systems.

Figure 6a provides further insight into the iterative behavior of HI-VQE compared to HCI. The energy convergence plot shows that HI-VQE approaches the CAS-CI benchmark within a few iterations, confirming the effectiveness of the handover mechanism between quantum sampling and classical diagonalization. Simultaneously, the subspace size remains significantly smaller for HI-VQE across all iterations (Figure 6b), even as the algorithm refines the wavefunction. This compactness directly translates into reduced diagonalization costs and improved scalability, which is critical for systems with large active spaces such as Fe–S clusters. Finally, Figure 7 tracks the energy error of HI-VQE relative to CAS-CI over successive iterations. The error decreases steadily and approaches the chemical accuracy, which validates the robustness of the hybrid approach in refining electronic structure, especially in Case 4, where the number of shots is increased to 100,000. By leveraging quantum sampling, HI-VQE achieves both accuracy and efficiency. These results underscore the potential of HI-VQE as a practical quantum–classical hybrid framework for tackling strongly correlated systems, paving the way for applications in bioinorganic chemistry, catalysis, and materials science.

The case-dependent behavior reported in Table 5 provides additional insight. Case 1 (EPA-L-R2, 50,000 shots) already reaches 0.83 mHa with ~63M determinants, outperforming single-reference baselines by orders of magnitude in accuracy and below the chemical accuracy level. The *ad hoc* circuit in Case 2 attains the same level of accuracy as Case 1 with ~71M determinants, indicating that physically motivated, excitation-preserving ansätze (EPA-L-R2) better exploit the structure of the Fe–S electronic manifold than non-number-conserving or less tailored circuits. When the 25,000 shots were applied (Case 3), HI-VQE could not reach the chemical accuracy within 22 iterations. Crucially, Case 4 reduces the calculations to 6 iterations and achieves an error of 0.92 mHa with 72M determinants, underscoring the role of sampling statistics in suppressing stochastic variance and enhancing determinant selection by increasing number of shot to 100,000 shots. Across these runs, the determinant savings relative to HCI (which requires 56.7–196.1M determinants to reach ≤ 1 mHa) are consistent and substantive, highlighting a clear computational advantage.

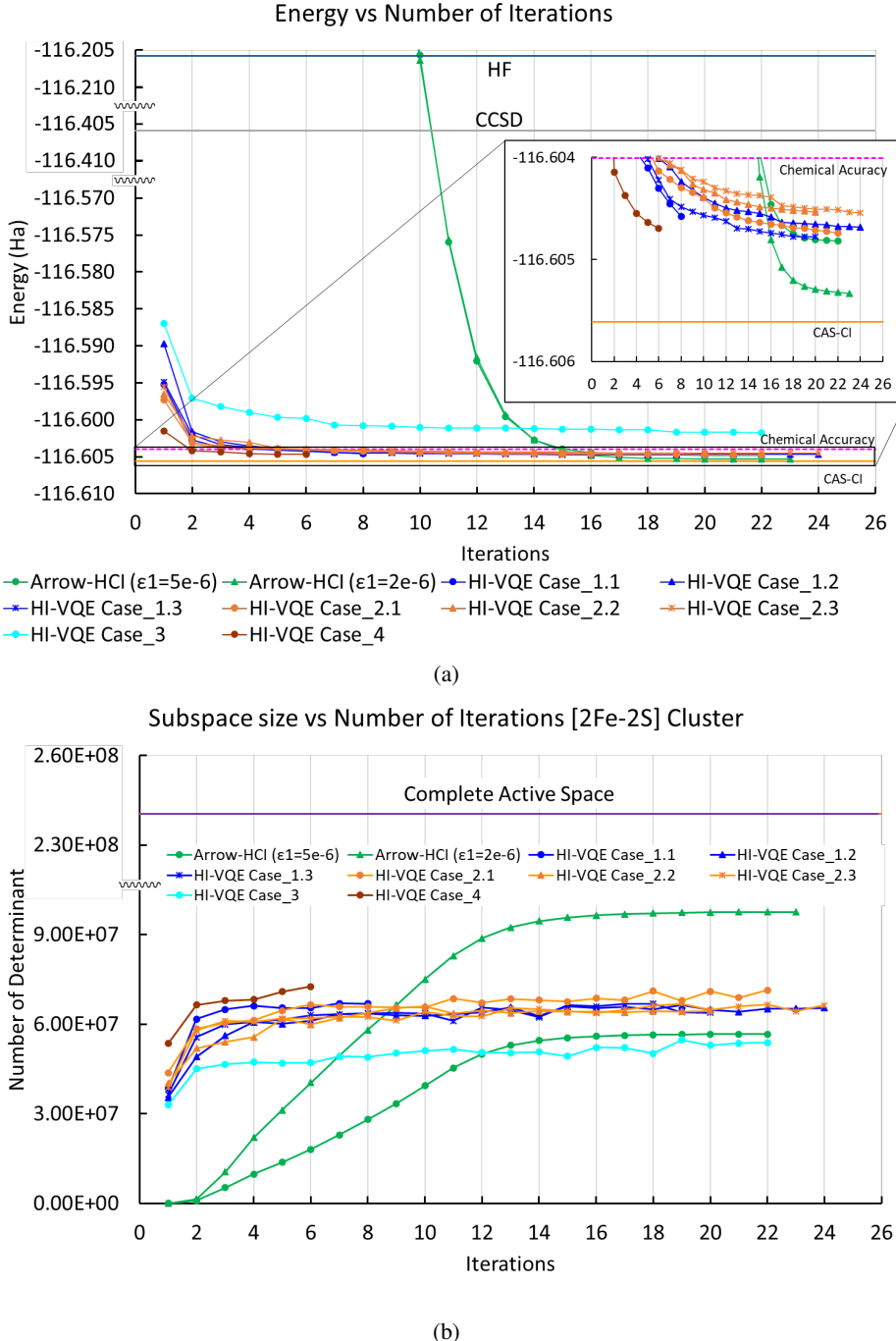


Figure 6: (a) The energy vs the number of iterations of [2Fe-2S] cluster (30e,20o) system using the TZP-DHK basis with 40 qubits. The HCI energy was taken from Ref. [29] and HI-VQE calculations. (b) The subspace size vs the number of iterations of each calculation

4 Conclusion

This study demonstrates that the HI-VQE can reliably extend quantum-classical hybrid simulation to the frontiers of strong electronic correlation. By benchmarking against state-of-the-art classical approaches, we showed that HI-VQE reproduces HCI-level energies for both the nitrogen molecule and the [2Fe-2S] cluster within millihartree accuracy. HI-VQE achieves chemical-accuracy-level agreement with classical HCI across the entire N_2 dissociation coordinate

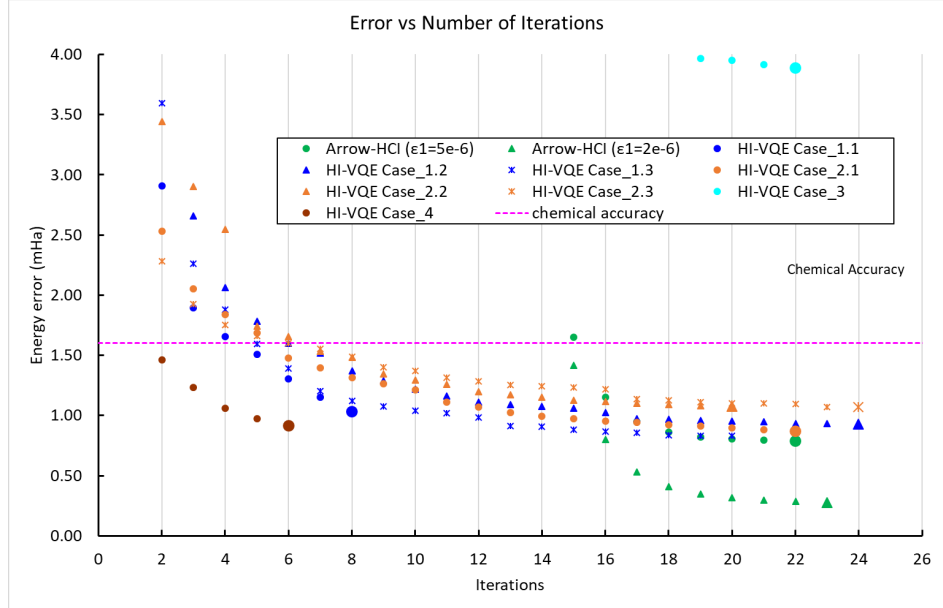


Figure 7: The energy error vs the number of iterations of [2Fe-2S] cluster (30e,20o) system using the TZP-DHK basis with 40 qubits with respect to the HCI energy taken from Ref. [29].

while requiring substantially fewer determinants and reduced computational resources than HCI, demonstrating that quantum-informed subspace expansion can outperform purely classical determinant selection even for multireference systems of realistic scale.

Beyond these benchmarks, the results establish HI-VQE as a practical framework for quantum-enhanced electronic-structure theory. Its iterative handover between quantum sampling and classical diagonalization provides a scalable route to treat localized and delocalized correlation on equal footing. As quantum processors mature, this approach offers a compelling path toward first-principles modeling of bioinorganic cofactors, catalytic reaction networks, and correlated materials that currently challenge classical computation. The present work thus marks a step toward the routine use of quantum resources in chemically and biologically meaningful simulations.

5 Acknowledgement

We acknowledge the use of IBM Quantum Credits for this work. The views expressed are those of the authors and do not reflect the official policy or position of IBM or the IBM Quantum Platform team. This research was conducted by the Research and Development team at Qunova Computing Inc. (Korea) and RIKEN (Japan). The authors declare that they have no conflicts of interest to disclose and would like to thank the developers of the open-source framework Qiskit, which was instrumental in implementing and benchmarking the HI-VQE algorithm for quantum simulation. All scientific content, interpretations, and conclusions are the sole responsibility of the authors.

References

- [1] P. A. M. Dirac, “Quantum mechanics of many-electron systems,” *Proceedings of the Royal Society of London. Series A, Containing Papers of a Mathematical and Physical Character*, vol. 123, no. 792, pp. 714–733, 1929.
- [2] W. E. Lamb and R. C. Rutherford, “Fine structure of the hydrogen atom by a microwave method,” *Physical Review*, vol. 72, no. 3, pp. 241–243, 1947.
- [3] T. Aoyama, N. Asmussen, T. Kinoshita, M. Nio, and M. Passera, “The anomalous magnetic moment of the electron: Status and perspectives,” *Physics Reports*, vol. 887, pp. 1–166, 2020.
- [4] T. Helgaker, P. Jørgensen, and J. Olsen, *Molecular Electronic-Structure Theory*. Chichester, UK: John Wiley & Sons, 2000.

[5] H. Gao, S. Imamura, A. Kasagi, and E. Yoshida, “Distributed implementation of full configuration interaction for one trillion determinants,” *Journal of Chemical Theory and Computation*, vol. 20, no. 3, pp. 1185–1192, Feb. 2024, publisher: American Chemical Society. [Online]. Available: <https://doi.org/10.1021/acs.jctc.3c01190>

[6] S. Kokott, F. Merz, Y. Yao, C. Carbogno, M. Rossi, V. Havu, M. Rampp, M. Scheffler, and V. Blum, “Efficient all-electron hybrid density functionals for atomistic simulations beyond 10,000 atoms,” *The Journal of Chemical Physics*, vol. 161, no. 2, p. 024112, 2024, survey and examples table summarizing hybrid-DFT calculations reaching thousands of atoms on HPC platforms (diverse international contributions).

[7] J. N. Harvey, “On the accuracy of density functional theory in transition metal chemistry,” *Annu. Rep. Prog. Chem., Sect. C: Phys. Chem.*, vol. 102, pp. 203–226, 2006. [Online]. Available: <http://dx.doi.org/10.1039/B419105F>

[8] L. Cao and U. Ryde, “Extremely large differences in dft energies for nitrogenase models,” *Physical Chemistry Chemical Physics*, vol. 21, no. 5, pp. 2480–2488, 2019.

[9] V. P. Vysotskiy, M. Torbjörnsson, H. Jiang, E. D. Larsson, L. Cao, U. Ryde, H. Zhai, S. Lee, and G. K.-L. Chan, “Assessment of dft functionals for a minimal nitrogenase $[\text{Fe}(\text{SH})_4\text{H}]^-$ model employing high-level wavefunction methods as reference,” *Physical Chemistry Chemical Physics*, vol. 22, pp. 17 487–17 500, 2020.

[10] I. W. Bulik, T. M. Henderson, and G. E. Scuseria, “Can single-reference coupled cluster theory describe static correlation?” *Journal of Chemical Theory and Computation*, vol. 11, pp. 3171–3179, 2015.

[11] K. Kowalski and P. Piecuch, “Renormalized CCSD(T) and CCSD(TQ) approaches: Dissociation of the N_2 triple bond,” *Journal of Chemical Physics*, vol. 113, no. 14, pp. 5644–5652, 2000.

[12] Y. Cao, J. Romero, J. P. Olson, M. Degroote, P. D. Johnson, M. Kieferová, I. D. Kivlichan, T. Menke, B. Peropadre, N. P. D. Sawaya, S. Sim, L. Veis, and A. Aspuru-Guzik, “Quantum chemistry in the age of quantum computing,” *Chemical Reviews*, vol. 119, no. 19, pp. 10 856–10 915, 2019, pMID: 31469277.

[13] R. A. Friesner, “*Ab initio* quantum chemistry: Methodology and applications,” *Proceedings of the National Academy of Sciences*, vol. 102, no. 19, pp. 6648–6653, 2005. [Online]. Available: <https://www.pnas.org/doi/abs/10.1073/pnas.0408036102>

[14] A. A. Holmes, N. M. Tubman, and C. Umrigar, “Heat-bath configuration interaction: An efficient selected configuration interaction algorithm inspired by heat-bath sampling,” *Journal of chemical theory and computation*, vol. 12, no. 8, pp. 3674–3680, 2016.

[15] S. Sharma, A. A. Holmes, G. Jeanmairet, A. Alavi, and C. J. Umrigar, “Semistochastic heat-bath configuration interaction method: Selected configuration interaction with semistochastic perturbation theory,” *Journal of chemical theory and computation*, vol. 13, no. 4, pp. 1595–1604, 2017.

[16] S. R. White, “Density matrix formulation for quantum renormalization groups,” *Phys. Rev. Lett.*, vol. 69, pp. 2863–2866, Nov 1992. [Online]. Available: <https://link.aps.org/doi/10.1103/PhysRevLett.69.2863>

[17] G. K.-L. Chan and M. Head-Gordon, “Highly correlated calculations with a polynomial cost algorithm: A study of the density matrix renormalization group,” *The Journal of Chemical Physics*, vol. 116, no. 11, pp. 4462–4476, 03 2002.

[18] G. K.-L. Chan and S. Sharma, “The density matrix renormalization group in quantum chemistry,” *Annual Review of Physical Chemistry*, vol. 62, pp. 465–481, 2011.

[19] W. Liu and M. R. Hoffmann, “iCI: Iterative CI toward full CI,” *Journal of chemical theory and computation*, vol. 12, no. 3, pp. 1169–1178, 2016.

[20] A. Menczer, M. van Damme, A. Rask, L. Huntington, J. Hammond, S. S. Xantheas, M. Ganahl, and O. Legeza, “Parallel implementation of the density matrix renormalization group method achieving a quarter petaflops performance on a single dgx-h100 gpu node,” *Journal of Chemical Theory and Computation*, vol. 20, no. 19, pp. 8397–8404, 2024.

[21] K. T. Williams, Y. Yao, J. Li, L. Chen, H. Shi, M. Motta, C. Niu, U. Ray, S. Guo, R. J. Anderson, J. Li, L. N. Tran, C.-N. Yeh, B. Mussard, S. Sharma, F. Bruneval, M. van Schilfgaarde, G. H. Booth, G. K.-L. Chan, S. Zhang, E. Gull, D. Zgid, A. Millis, C. J. Umrigar, and L. K. Wagner, “Direct comparison of many-body methods for realistic electronic hamiltonians,” *Physical Review X*, vol. 10, no. 1, p. 011041, 2020.

[22] J. Preskill, “Quantum computing in the nisq era and beyond,” *Quantum*, vol. 2, p. 79, 2018. [Online]. Available: <https://doi.org/10.22331/q-2018-08-06-79>

[23] F. Arute, K. Arya, R. Babbush *et al.*, “Quantum supremacy using a programmable superconducting processor,” *Nature*, vol. 574, no. 7779, pp. 505–510, 2019. [Online]. Available: <https://doi.org/10.1038/s41586-019-1666-5>

[24] M. Kjaergaard, M. E. Schwartz, J. Braumüller, P. Krantz, J. I.-J. Wang, S. Gustavsson, and W. D. Oliver, “Superconducting qubits: Current state of play,” *Annual Review of Condensed Matter Physics*, vol. 11, pp. 369–395, 2020. [Online]. Available: <https://doi.org/10.1146/annurev-conmatphys-031119-050605>

[25] J. R. McClean, J. Romero, R. Babbush, and A. Aspuru-Guzik, “The theory of variational hybrid quantum-classical algorithms,” *New Journal of Physics*, vol. 18, no. 2, p. 023023, 2016.

[26] M. Cerezo, A. Arrasmith, R. Babbush, S. C. Benjamin, S. Endo, K. Fujii, J. R. McClean, K. Mitarai, X. Yuan, L. Cincio, and P. J. Coles, “Variational quantum algorithms,” *Nature Reviews Physics*, vol. 3, pp. 625–644, 2021.

[27] K. Bharti, A. Cervera-Lierta, T. H. Kyaw, T. Haug, S. Alperin-Lea, A. Anand, M. Degroote, H. Heimonen, J. S. Kottmann, T. Menke, W. K. Mok, S. Sim, L.-C. Kwek, and A. Aspuru-Guzik, “Noisy intermediate-scale quantum algorithms,” *Reviews of Modern Physics*, vol. 94, no. 1, p. 015004, 2022.

[28] A. Peruzzo, J. McClean, P. Shadbolt, M.-H. Yung, X.-Q. Zhou, P. J. Love, A. Aspuru-Guzik, and J. L. O’Brien, “A variational eigenvalue solver on a photonic quantum processor,” *Nature Communications*, vol. 5, no. 1, p. 4213, Jul. 2014, publisher: Nature Publishing Group. [Online]. Available: <https://www.nature.com/articles/ncomms5213>

[29] J. Robledo-Moreno, M. Motta, H. Haas, A. Javadi-Abhari, P. Jurcevic, W. Kirby, S. Martiel, K. Sharma, S. Sharma, T. Shirakawa, I. Sitzdikov, R.-Y. Sun, K. J. Sung, M. Takita, M. C. Tran, S. Yunoki, and A. Mezzacapo, “Chemistry beyond the scale of exact diagonalization on a quantum-centric supercomputer,” *Science Advances*, vol. 11, p. eadu9991, 2025.

[30] H. R. Grimsley, S. E. Economou, E. Barnes, and N. J. Mayhall, “An adaptive variational algorithm for exact molecular simulations on a quantum computer,” *Nature Communications*, vol. 10, no. 1, p. 3007, Jul. 2019, publisher: Nature Publishing Group. [Online]. Available: <https://www.nature.com/articles/s41467-019-10988-2>

[31] J. Tilly, H. Chen, S. Cao, D. Picozzi, K. Setia, Y. Li, E. Grant, L. Wossnig, I. Rungger, G. H. Booth, and J. Tennyson, “The variational quantum eigensolver: A review of methods and best practices,” *Physics Reports*, vol. 986, pp. 1–128, 2022.

[32] T. Shirakawa, J. Robledo-Moreno, T. Itoko, V. Tripathi, K. Ueda, Y. Kawashima, L. Broers, W. Kirby, H. Pathak, H. Paik, M. Tsuji, Y. Kodama, M. Sato, C. Evangelinos, S. Seelam, R. Walkup, S. Yunoki, M. Motta, P. Jurcevic, H. Horii, and A. Mezzacapo, “Closed-loop calculations of electronic structure on a quantum processor and a classical supercomputer at full scale,” 2025. [Online]. Available: <https://arxiv.org/abs/2511.00224>

[33] A. Pellow-Jarman, S. McFarthing, D. H. Kang, P. Yoo, E. E. Elala, R. Pellow-Jarman, P. M. Nakliang, J. Kim, and J.-K. K. Rhee, “Hivqe: Handover iterative variational quantum eigensolver for efficient quantum chemistry calculations,” 2025. [Online]. Available: <https://arxiv.org/abs/2503.06292>

[34] S. Sharma, K. Sivalingam, F. Neese, and G. K.-L. Chan, “Low-energy spectrum of iron-sulfur clusters directly from many-particle quantum mechanics,” *Nature Chemistry*, vol. 6, pp. 927–933, 2014.

[35] Z. Li and G. K.-L. Chan, “Spin-projected matrix product states: Versatile tool for strongly correlated systems,” *Journal of Chemical Theory and Computation*, vol. 13, pp. 2681–2695, 2017.

[36] (2024) Sqd data repository. GitHub. [Online]. Available: https://github.com/jrm874/sqd_data_repository/tree/main/integrals

[37] J. Li, M. Otten, A. A. Holmes, S. Sharma, and C. J. Umrigar, “Fast semistochastic heat-bath configuration interaction,” *J. Chem. Phys.*, vol. 148, p. 214110, 2018.

[38] P. Åke Malmqvist and B. O. Roos, “The casscf state interaction method,” *Chemical Physics Letters*, vol. 155, no. 2, pp. 189–194, 1989. [Online]. Available: <https://www.sciencedirect.com/science/article/pii/0009261489853473>

[39] G. H. Booth, D. Cleland, A. J. W. Thom, and A. Alavi, “Breaking the carbon dimer: The challenges of multiple bond dissociation with full configuration interaction quantum monte carlo methods,” *The Journal of Chemical Physics*, vol. 135, no. 8, p. 084104, 08 2011.

[40] V. Rishi, A. Perera, and R. J. Bartlett, “Assessing the distinguishable cluster approximation based on the triple bond-breaking in the nitrogen molecule,” *The Journal of Chemical Physics*, vol. 144, no. 12, p. 124117, 03 2016.

[41] D. Kats, “Communication: The distinguishable cluster approximation. ii. the role of orbital relaxation,” *The Journal of Chemical Physics*, vol. 141, no. 6, p. 061101, 08 2014. [Online]. Available: <https://doi.org/10.1063/1.4892792>

[42] A. J. Cohen, P. Mori-Sánchez, and W. Yang, “Fractional spins and static correlation error in density functional theory,” *Journal of Chemical Physics*, vol. 129, no. 12, p. 121104, 2008.

[43] J.-N. Boyn and D. A. Mazziotti, “Elucidating the molecular orbital dependence of the total electronic energy in multireference problems,” *Journal of Chemical Physics*, vol. 156, no. 19, p. 194104, 2022.

[44] D. C. Frost and C. A. McDowell, “The dissociation energy of the nitrogen molecule,” *Proceedings of the Royal Society of London. Series A. Mathematical and Physical Sciences*, vol. 236, no. 1205, pp. 278–284, 1956. [Online]. Available: <https://royalsocietypublishing.org/doi/abs/10.1098/rspa.1956.0135>

[45] P. Wang, S. Gong, Y. Li, and Y. Mo, “Bond dissociation energy of n₂ measured by state-to-state resolved threshold fragment yield spectra,” *The Journal of Chemical Physics*, vol. 160, no. 1, p. 014304, 01 2024. [Online]. Available: <https://doi.org/10.1063/5.0187003>

[46] M. Ball and M. Head-Gordon, “Electronic structure of strongly correlated systems: recent developments in multiconfiguration pair-density functional theory and multiconfiguration n-electron valence state perturbation theory,” *Chemical Science*, vol. 13, pp. 7685–7706, 2022.

[47] H. Beinert, R. H. Holm, and E. Münck, “Iron-sulfur clusters: Nature’s modular, multipurpose structures,” *Science*, vol. 277, pp. 653–659, 1997. [Online]. Available: <https://pubmed.ncbi.nlm.nih.gov/25242489/>

[48] M. Zhang, Z. Liu, Y. Le, Z. Gu, and H. Zhao, “Iron-sulfur clusters: A key factor of regulated cell death in cancer,” *Oxidative Medicine and Cellular Longevity*, vol. 2022, p. 7449941, 2022.

[49] H. Zhai, S. Lee, Z. H. Cui, L. Cao, U. Ryde, and G. K.-L. Chan, “Multireference protonation energetics of a dimeric model of nitrogenase iron–sulfur clusters,” *Journal of Physical Chemistry A*, vol. 127, no. 47, pp. 9974–9984, 2023.

[50] L. Hehn, P. Deglmann, and M. Kühn, “Assessing electronic-structure methods for redox potentials of an iron-sulfur cluster,” *International Journal of Quantum Chemistry*, vol. 125, p. e70068, 2025.

[51] S. Zhou, D. Liu, K. Fan, H. Liu, and X.-D. Zhang, “Atomic-level design of biomimetic iron–sulfur clusters for biocatalysis,” *Nanoscale*, vol. 16, pp. 18 644–18 665, 2024. [Online]. Available: <http://dx.doi.org/10.1039/D4NR02883J>

[52] B. Benediktsson and R. Bjornsson, “Analysis of the geometric and electronic structure of spin-coupled iron–sulfur dimers with broken-symmetry DFT: Implications for FeMoco,” *Journal of Chemical Theory and Computation*, vol. 18, no. 3, pp. 1437–1457, 2022.

[53] V. P. Vysotskiy, M. Torbjörnsson, H. Jiang, E. D. Larsson, L. Cao, U. Ryde, H. Zhai, S. Lee, and G. K.-L. Chan, “Scalar relativistic all-electron and pseudopotential ab initio study of a minimal nitrogenase FeSH₄H[−] model employing coupled-cluster and auxiliary-field quantum monte carlo many-body methods,” *Journal of Physical Chemistry A*, 2024, see text; DOI/volume/pages as published. [Online]. Available: <https://ris.utwente.nl/ws/portalfiles/portal/369032796/vysotskiy-et-al-2024-scalar-relativistic-all-electron-and-pseudopotential-ab-initio-study-of-a-minimal-nitrogenase.pdf>

[54] Y. Yao and C. Umrigar, “Orbital optimization in selected configuration interaction methods,” *Journal of Chemical Theory and Computation*, vol. 17, no. 7, pp. 4183–4194, 2021.

[55] V. Abraham and N. J. Mayhall, “Cluster many-body expansion: A many-body expansion of the electron correlation energy about a cluster mean field reference,” *The Journal of Chemical Physics*, vol. 155, no. 5, p. 054101, 08 2021. [Online]. Available: <https://doi.org/10.1063/5.0057752>